

First-Principles Study of the Temperature Dependence of Structural, Electronic, and Hyperfine Properties of the Cu(100) Surface

Germán N. Darriba^{1,*}, R. Faccio² and Mario Rentería^{1,*}

¹ *Departamento de Física “Prof. Dr. Emil Bose” and Instituto de Física La Plata [IFLP, Consejo Nacional de Investigaciones Científicas y Técnicas (CONICET) La Plata], Facultad de Ciencias Exactas, Universidad Nacional de La Plata, CC 67, (1900) La Plata, Argentina.*

² *Área Física y Centro NanoMat, DETEMA, Facultad de Química, Universidad de la República, Gral. Flores 2124, P.O. Box 1157, Montevideo, Uruguay.*

ABSTRACT

In this work, we investigate the temperature-dependent behavior of the pure (undoped) Cu(100) surface using first-principles calculations within the Density Functional Theory framework. One of the main objectives is to determine whether the linear dependence of the predicted electric-field gradient (EFG) tensor on the outermost Cu atom on the Cu(100) surface arises from the same generation of the surface or from the reconstruction of the surface. To this end, we perform here a comprehensive *ab initio* study of the Cu(100) surface reconstruction and its associated structural, electronic, and hyperfine properties as a function of temperature, not only at the outermost atomic layer (i.e., the topmost Cu atom) but also as a function of atomic depth relative to the reconstructed surface. To study the temperature dependence of the EFG, we use experimentally determined temperature-dependent lattice parameters for bulk copper in our calculations. The anisotropic relaxation that arises when bulk symmetry is broken helps unravel the potential sources of EFG temperature dependence at the surface. Studying the electron density of conduction electrons $\rho(\vec{r})$ at the atomic scale near the Cu nucleus and the atom-resolved partial density of states at the topmost Cu atom allows us to correlate the surface effect on the EFG with the bulk value. Finally, we correlate the temperature dependence of the EFG on the undoped Cu(100) surface with the linear behavior of the “ionic” contribution to the EFG.

INTRODUCTION

The atomic-scale geometric configuration at and near solid surfaces plays a pivotal role in understanding interatomic and interlayer interactions under these boundary conditions. When surfaces are generated, several new physical properties that are not exhibited in bulk materials can emerge, significantly influencing their behavior and potential technological applications [1]-[5].

Surface formation inherently breaks the bulk crystal's translational symmetry, generating stress fields that drive structural relaxation and reconstruction toward new equilibrium configurations. These *reconstructed* surfaces often exhibit distinct electronic and magnetic properties compared with their bulk counterparts, making their characterization essential for both fundamental and applied research.

Hyperfine interactions with suitable radioactive probe atoms are a powerful tool for studying atomic environments and electronic and magnetic properties in solids. Magnetic dipole and electric quadrupole hyperfine couplings provide insight into exchange interactions and the spatial distribution of electron charge density surrounding atomic probe nuclei. In particular, the electric-field gradient (EFG) tensor at the site of the probe nucleus is highly sensitive to the anisotropy of the local electronic environment due to its inverse-cubic dependence on the radial coordinate, r^{-3} . The EFG components are defined as $V_{ij}(\vec{r}) = \frac{\partial^2 V(\vec{r})}{\partial x_i \partial x_j}$, where $V(\vec{r})$ is the electrostatic potential. In its principal axis system, the diagonalized EFG tensor (being traceless) is fully characterized by its largest principal component V_{33} and the asymmetry parameter $\eta = \frac{V_{11} - V_{22}}{V_{33}}$, with the convention standard $|V_{11}| \leq |V_{22}| \leq |V_{33}|$, reflecting the local electron density anisotropy. The highly precise experimental measurement of this tensor, combined with reliable EFG calculations, can offer comprehensive insight into the electron density (represented as $\rho(\vec{r})$) of the system being investigated or designed. The EFG at a probe nucleus is determined with high precision using the time-differential perturbed γ - γ angular correlations (TDPAC) spectroscopy. This technique measures the nuclear quadrupole frequency ω_Q of the hyperfine interaction between the EFG tensor and the nuclear quadrupole moment Q of the probe's sensitive nuclear state. Then, V_{33} is determined through $\omega_Q = eQV_{33}/40\hbar$ (for the most widely used ^{111}Cd probe studied here), provided the quadrupole moment Q is known. Comprehensive

descriptions of TDPAC principles and experimental measurements can be found in Refs. [6]-[9].

On FCC metal surfaces, numerous experimental [10]-[17] and first-principles [18] studies have investigated the EFG at substitutional sites of diluted ^{111}Cd probe atoms located at the topmost atomic positions, a measurement that is experimentally challenging. However, only a few of these surfaces have been studied experimentally as a function of measurement temperature. In particular, the study of deposited $^{111}\text{In}(\rightarrow^{111}\text{Cd})$ impurities on the Cu(100) surface, using TDPAC spectroscopy, reveals a strong linear temperature dependence of the EFG [10]. The relative decrease of V_{33} shown across a temperature range from 0 to 1000 K, $\frac{V_{33}(1000\text{ K})-V_{33}(0\text{ K})}{V_{33}(0\text{ K})}$, gives 10.5 %. Due to the cubic symmetry of the Cu FCC lattice, the EFG in the bulk is zero, making a direct comparison (in % of change) between bulk and surface behavior impossible. On the other hand, for many bulk materials with noncubic metallic structures (thus with nonnull EFGs), the bulk EFG has a $-\alpha T^{3/2}$ dependence ($\alpha > 0$) [19], with the mean-square displacement of probe atoms and their immediate neighbors responsible for this effect.

In this work, we investigate the temperature-dependent behavior of the pure (undoped) Cu(100) surface using first-principles calculations within the Density Functional Theory (DFT) framework. One of the main goals is to enlighten whether the previously observed linear dependence of the EFG at the ^{111}Cd -doped Cu(100) surface [1] arises intrinsically during surface formation and reconstruction, is induced by the Cd impurity's electronic configuration, its deformation, and the local structural relaxation it produces, or is the result of all these effects. To this end, and as a first step toward a more complex future study of the doped surface, we perform here a comprehensive *ab initio* study of the Cu(100) surface reconstruction and its associated structural, electronic, and hyperfine properties as a function of temperature, not only at the outermost atomic layer (i.e., the topmost Cu atom) but also as a function of atomic depth relative to the reconstructed surface.

Understanding surface reconstruction and studying the EFG behavior at all Cu sites as a function of temperature, using experimentally determined temperature-dependent lattice parameters for bulk copper in our calculations and accounting for anisotropic relaxation that arises when bulk symmetry is broken, helps unravel the potential sources of EFG temperature dependence at the doped surface. Additionally,

studying the electron density of conduction electrons at the atomic scale near the Cu nucleus and the atom-resolved partial electronic density of states (PDOS) at the topmost Cu atom allows us to correlate the surface effect on the EFG with the bulk value. Finally, we can correlate the temperature dependence of the EFG on the undoped Cu(100) surface with the linear behavior of the “ionic” contribution to the EFG.

METODOLOGY

To simulate the Cu(001) surface, we employ the slab-supercell (SC) approach, starting from the FCC bulk system, as shown in Fig. 1. We use a slab containing seven inequivalent substrate atomic layers, since this size (13 layers per SC) is sufficient to obtain a bulk-like environment at the deepest Cu atoms. In addition, we considered up to 11 inequivalent substrate layers to check size convergence. The thickness of the vacuum region between adjacent slabs was set to approximately 10 Å to prevent electronic coupling between the slabs. We call the *just-generated surface* the SC without any relaxation of its atomic positions, and therefore, the forces at Cu atoms are much stronger as the Cu atom approaches the surface. Consequently, we performed a complete relaxation of the atomic positions in the just-generated SC, yielding the equilibrium structure and the *reconstructed surface*. The notation Cu_i ($i = 1-7$) refers to Cu atoms from the surface to the bulk, with Cu_1 being the topmost Cu atom and Cu_7 the deepest one. To account for thermal effects, we use experimentally determined lattice parameters for Cu bulk as a function of temperature over the 20-1350 K range [20]. Using these parameters, we begin by obtaining the reconstructed surface from the just-generated one at 20 K. At these structural equilibrium positions, we adjust the lattice parameters to those corresponding to the next higher temperature and perform a complete relaxation again, yielding a new reconstructed surface for that temperature. This procedure is repeated, increasing the temperature until the parameters corresponding to the highest temperature are used, as in an experiment in which the measurement temperature is increased gradually. For verification, we also relaxed the just-generated SCs obtained using the lattice parameters at each temperature. The V_{33} values obtained in this way at the Cu_1 atom were very similar to those obtained with the previous procedure.

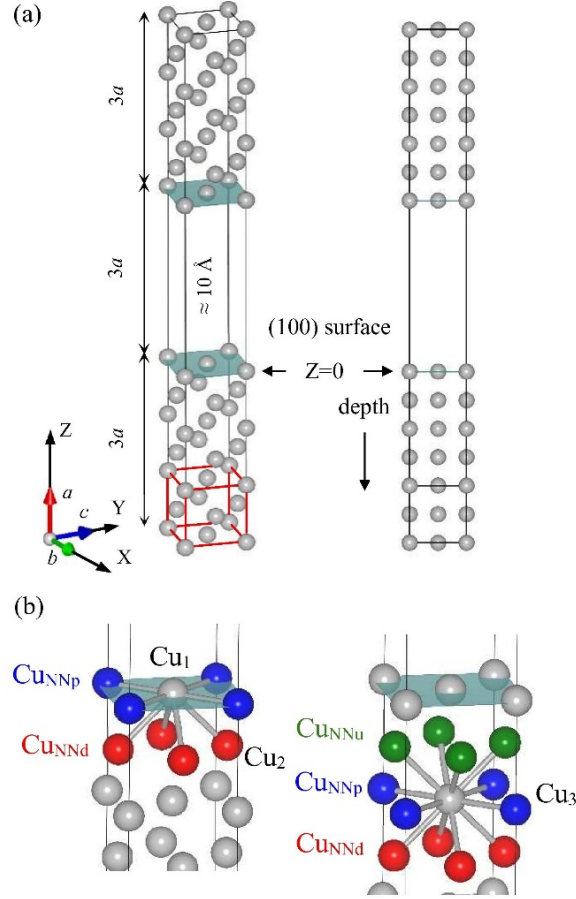


Figure 1. (a) Slab-super-cell containing seven inequivalent substrate layers (13 atomic layers in total), used to simulate the Cu(100) surface. The FCC cell is shown in red. Crystalline axes and principal axis system of the diagonalized EFG are shown. (b) Zoom of the surface region. Left: the eight Cu_{NN} atoms to Cu_1 are divided into four Cu_{NNp} in the same surface plane (blue atoms) and four Cu_{NNd} in the lower layer plane (red atoms). Right: the twelve Cu_{NN} atoms to Cu_3 are divided into four Cu_{NNp} in the same layer plane (blue atoms), four Cu_{NNd} in the lower layer plane (red atoms), and four Cu_{NNu} in the upper layer plane (green atoms).

For the present study, we use state-of-the-art first-principles calculations within the framework of DFT [21] [22], employing the full-potential augmented plane wave plus local orbitals (APW+lo) method [23], implemented in the WIEN2k package [24]. Here, the exchange-correlation effects were treated using the Perdew-Burke-Ernzerhof (PBE-GGA) parametrization [25]. The cutoff parameter of the plane-wave basis is $R_{\text{MT}}K_{\text{max}} = 7$, where R_{MT} and K_{max} are the chosen radius of the nonoverlapping muffin-

tin Cu spheres and the greatest modulus of the lattice vectors in reciprocal space, respectively. We take the radius of the sphere centered on the Cu atom to be $R_{\text{MT}}(\text{Cu}) = 1.17 \text{ \AA}$. The tetrahedron method [26] was used to integrate in reciprocal space, taking a k -space grid of $14 \times 14 \times 2$. Finally, the equilibrium structures for all calculations were obtained using a Newton-damped scheme until the forces on the ions were below 0.01 eV/\AA , and the EFG tensors were computed from the second derivative of the full electric potential evaluated for the final equilibrium structures [27], [28].

RESULTS AND DISCUSSION

In this section, we study the structural, electronic, and hyperfine properties of the *just-generated* and *reconstructed* Cu(100) surfaces with the aim of contributing to elucidating the unexpected linear temperature dependence of the EFG for deposited ($^{111}\text{In} \rightarrow$) ^{111}Cd impurities on the Cu(100) surface [1]. In this first stage, we isolate the effects arising solely from the surface boundary conditions.

Due to these boundary conditions, only the topmost Cu atom (Cu_1) has eight Cu atoms as nearest neighbors: four (Cu_{NNp}) in the same surface plane and four (Cu_{NNd}) in the lower layer (see Fig. 1(b), left). The remaining Cu_i atoms (i from 2 to 7) have twelve nearest neighbors: four in the same plane (Cu_{NNp}), four in the lower layer (Cu_{NNd}), and four in the upper layer (Cu_{NNu}), as in bulk FCC copper. This coordination is illustrated for the Cu_3 atom on the right-hand side of Fig. 1(b).

When the surface reaches its equilibrium structure, the system relaxes, and the distances between each inequivalent Cu_i atom and its nearest neighbors change. In Fig. 2, we plot the distance $d(\text{Cu}_i\text{-Cu}_{\text{NN}})$ between each inequivalent Cu_i atom in the SC and its neighbors as a function of temperature for the *just-generated surface* (hollow squares) and the *reconstructed surface* after the converged full relaxation (triangles and circles).

As shown, for all inequivalent Cu_i atoms, the distances to the Cu_{NNp} atoms, which lie in the same plane as Cu_i , remain unchanged as the structure relaxes (at 0 K) to the *reconstructed surface*, i.e., the atomic positions of the bulk system for these four Cu_{NNp} atoms are preserved. This will not be the case for the coordinated atoms outside this plane when the system relaxes. Also, the $d(\text{Cu}_i\text{-Cu}_{\text{NNp}})$ distances (and angles)

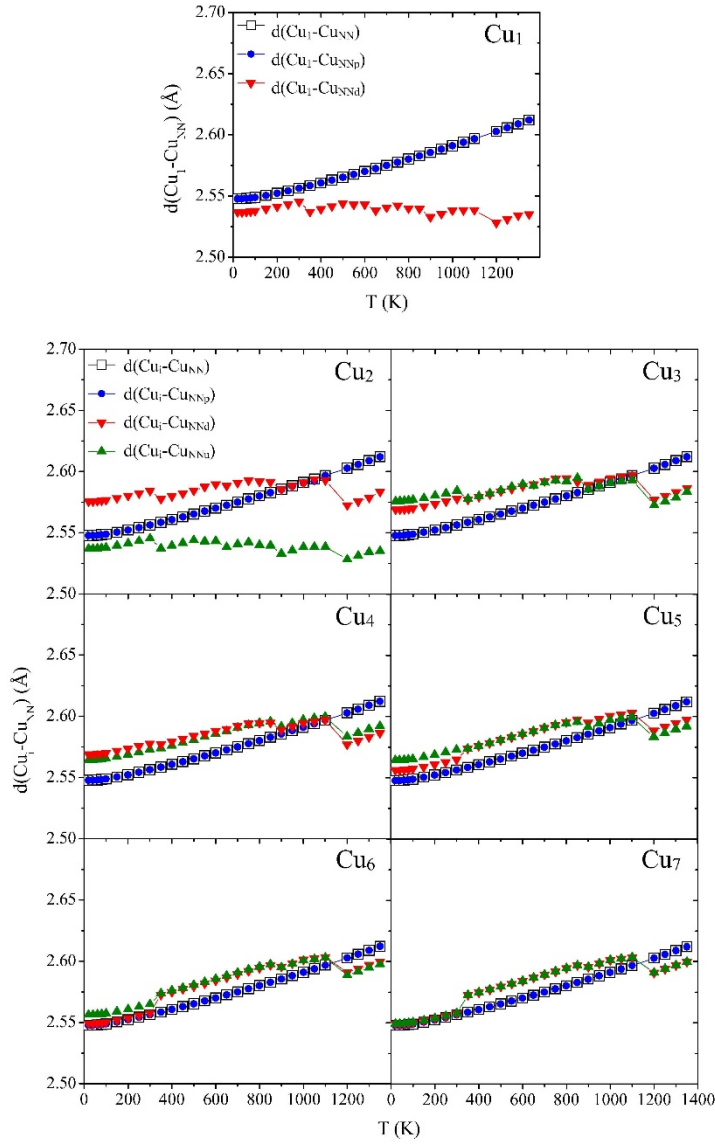


Figure 2. Distance $d(\text{Cu}_i\text{-Cu}_{\text{NN}})$ for each inequivalent Cu_i atom in the SC for the *just-generated* surface (hollow squares) and the *reconstructed* surface (triangles and circles), as a function of temperature (up: $i=1$, and down: i from 2 to 7). The blue circles and red and green triangles correspond to Cu_{NN} on the same plane and on the lower- and upper-layer planes relative to the Cu_i plane, respectively.

exhibit the same isotropic temperature dependence as in the bulk (blue circles and hollow squares are superimposed for all temperatures).

The Cu_1 atom is the only one without nearest-neighbor atoms above it. The $d(\text{Cu}_1\text{-Cu}_{\text{NNd}})$ distance is lower for the *reconstructed* surface than for the *just-generated* one at all temperatures. For temperatures greater than 300 K, this distance is practically

constant, in contrast to the behavior of $d(\text{Cu}_1\text{-Cu}_{\text{NNp}})$. In fact, there is a small accordion effect superimposed on the nearly constant temperature dependence of this bond length. This effect should arise from the interplay between the (nonlinear) lattice-parameter expansion and the linear contraction of the distance between the surface and the 2nd atomic layer, as we explain below.

Cu_2 is the atom in the layer just below the surface. For this atom, the behavior of $d(\text{Cu}_2\text{-Cu}_{\text{NNu}})$ and $d(\text{Cu}_2\text{-Cu}_{\text{NNd}})$ as temperature increases is essentially the same, with the difference that $d(\text{Cu}_2\text{-Cu}_{\text{NNu}})$ is smaller than $d(\text{Cu}_2\text{-Cu}_{\text{NNp}})$, whereas $d(\text{Cu}_2\text{-Cu}_{\text{NNd}})$ is greater than, equal to, and smaller than $d(\text{Cu}_2\text{-Cu}_{\text{NNp}})$ from 20 to 900 K, from 900 to 1100 K, and from 1100 to 1350 K, respectively. As the Cu_i atom moves away from the surface, i.e., from $i=3$ to $i=7$, the $d(\text{Cu}_i\text{-Cu}_{\text{NNu}})$ and $d(\text{Cu}_i\text{-Cu}_{\text{NNd}})$ tend toward $d(\text{Cu}_i\text{-Cu}_{\text{NNp}})$, becoming equal, as in Cu bulk, for Cu_7 from 20 to 300 K, and practically the same (difference less than 10^{-2} Å) for temperatures larger than 300 K, indicating the reconstruction of the bulk environment.

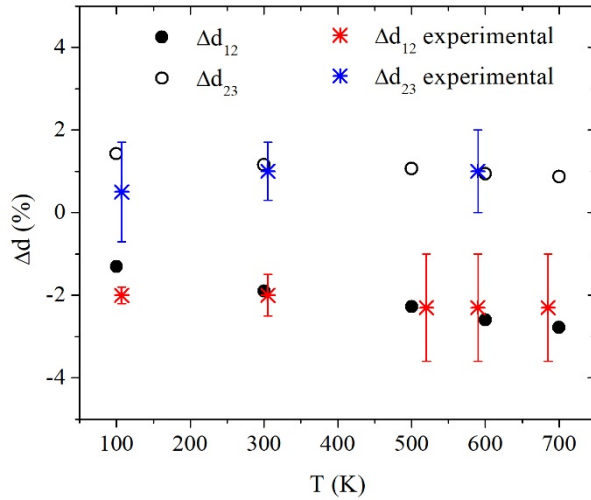


Figure 3. Predicted relative displacement Δd of the topmost (Δd_{12}) and second (Δd_{23}) interlayer distance as a function of temperature for the *reconstructed* surface, with respect to the interlayer distance in Cu bulk at each temperature. The experimental data come from Ref. [29].

Figure 3 plots the relative variation Δd of the topmost (Δd_{12}) and second (Δd_{23}) interlayer distance as a function of temperature for the *reconstructed* surface, with

respect to the interlayer distance in Cu bulk at each temperature. A positive (negative) value of Δd indicates expansion (contraction) of the interlayer distance upon relaxation at each higher temperature. In general, the topmost 1-2 interlayer distance contracts, while the second 2-3 interlayer distance expands relative to the bulk value, in excellent agreement with experimental determinations [29], pointing to a good description of the *reconstructed* surface. The bond length $d(\text{Cu}_1\text{-Cu}_{\text{NNd}})$, smaller than the bulk values (Fig. 2, up), is consistent with the contraction of the 1-2 interlayer of the *reconstructed surface*, already at 0 K. This bond length constant dependency on temperature (see Fig. 2) indicates that, while the 1-2 interlayer distance decreases, the angles of these bonds relative to the surface plane also decrease. Contrarily, the expansion of the 2-3 interlayer enables the expansion of the bond length $d(\text{Cu}_2\text{-Cu}_{\text{NNd}})$ at low temperatures relative to the bulk value and also remains rather constant with temperature (presenting a similar accordion effect as in $d(\text{Cu}_2\text{-Cu}_{\text{NNu}})$). The 2-3 initially expanded interlayer spacing decreases slightly as temperature increases.

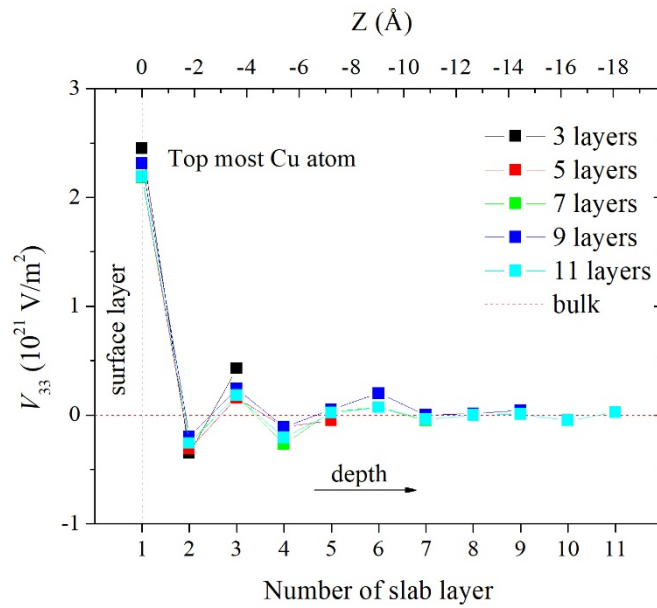


Figure 4. Predicted V_{33} value as a function of the depth of the Cu atom from the Cu(100) surface, for different numbers of inequivalent atomic slab layers used in the calculations at 300 K (from 3 to 11 inequivalent layers, indicated with different colors). The dashed red line represents the V_{33} value for the Cu bulk. $Z = 0 \text{ \AA}$ is the position of the topmost Cu atom in the *reconstructed* Cu(100) surface.

We now present the predicted EFG values. Figure 4 shows the V_{33} values (the largest component of the diagonalized EFG tensor) at Cu_i atoms at different depths (Z) and as a function of the number i of inequivalent atomic slab layers used in the *reconstructed* Cu(100) surface, using Cu lattice parameters at 300K. As shown, Cu_7 atoms located seven slab layers below the Cu(100) surface ($Z \approx 11 \text{ \AA}$) exhibit a null V_{33} value, recovering the bulk FCC symmetry of their environment and no longer experiencing the surface. For all EFG calculations at each Cu_i atom, we obtained $\eta_i=0$ (axial symmetry), and V_{33} is in the [100] direction (i.e., perpendicular to the surface). Consequently, all remaining *ab initio* results presented here were obtained using a slab with seven inequivalent atomic layers.

As shown in Fig. 4, there are essentially two values for V_{33} , one ($V_{33}^{Surface}$) for the topmost Cu_1 atom and another (V_{33}^B) for the remaining Cu_i atoms (from $i=2$ to 7) located below the surface. Comparing V_{33} at Cu atoms in the 2nd and 3rd layers with that of the topmost Cu_1 atom at the surface yields a factor of approximately 2. We cannot compare $V_{33}^{Surface}$ to the bulk value because it is null; however, a significant increase in V_{33} , with approximately a factor of 5, was experimentally observed at ^{111}Cd probes on the In(111) metallic surface relative to its bulk value [30]. A thorough inspection of the electron densities shown in Fig. 5 is representative and visually explains the increase in V_{33} from the bulk to the Cu(100) surface. This figure shows the electron density $\rho(\vec{r})$ at the (010) and (100) planes containing the topmost Cu_1 atom and the deepest Cu_7 atom in the *reconstructed* surface, for the most energetic (conduction) electron, calculated at 300 K. The critical angle $\theta_c = 54.7^\circ$ (Fig. 5, up), measured from the V_{33} axis, separates regions of negative charge that contribute to V_{33} with opposite signs [see Eq. (14) of Ref. [31] for details]: negative charge localized below θ_c (in fact, a conical region in three dimensions with V_{33} as its symmetry axis) contributes to V_{33} with negative values, and vice versa. At Cu_7 , the four elongated spots contribute to V_{33} with both positive and negative signs, canceling each other. At the surface, the spatial distribution of this negative charge at Cu_1 changes strongly, with almost all the charge distributed with axial symmetry around the V_{33} axis and located in the (100) plane ($\theta \approx 90^\circ$), thus contributing to a *large positive* EFG, in contrast to the almost null value at the Cu_7 atom.

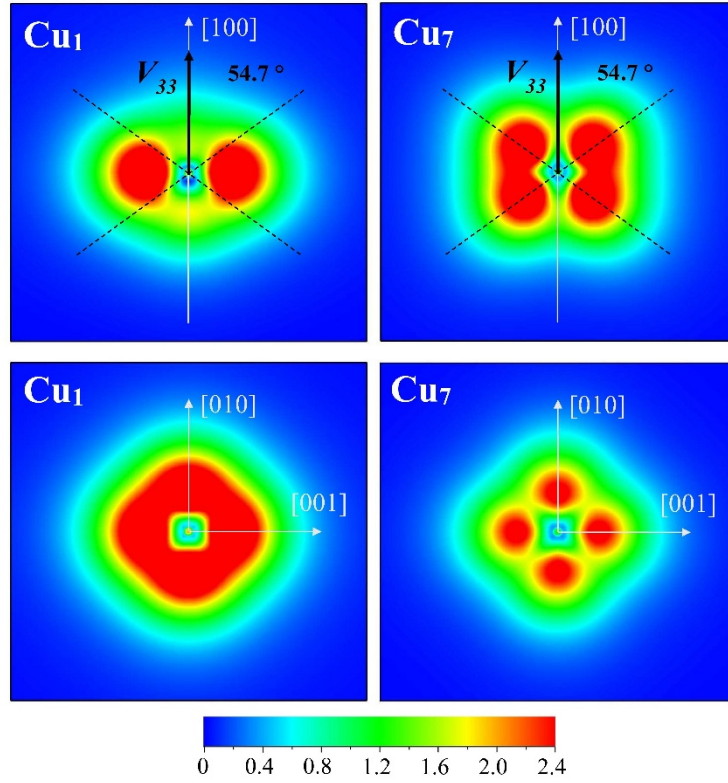


Figure 5. Electron density $\rho(\vec{r})$ at the (010) (up) and (100) (bottom) planes containing the topmost Cu₁ atom and the deepest Cu₇ atom of the *reconstructed* Cu(100) surface, for the most energetic (conduction) electron at 300 K.

We chose to first discuss the origin of the EFG at the surface using the last electron for several reasons. In the EFG parametrization for noncubic metals proposed by Raghavan *et al.* [31], [32], [7], the conduction-electron contribution to V_{33} has about two to three times the magnitude of the rest of the EFG sources. In effect, this parametrization proposes:

$$V_{33}^{tot} = V_{33}^{ionic} + V_{33}^{elect} = (1 - \gamma_{\infty})V_{33}^{latt} + V_{33}^{elect}. \quad (1)$$

In Eq. 1, the *ionic* contribution comes from the external EFG produced at the probe nucleus from the rest of the atoms of the crystal lattice, V_{33}^{latt} , plus another term arising from the antishielding effect of V_{33}^{latt} produced by the probe's filled electronic core shells, $-\gamma_{\infty} V_{33}^{latt}$. And V_{33}^{elect} is the *electronic* contribution arising from conduction electrons. If the empirical “universal correlation” [31], [32], [7] found for many noncubic metals applies for Cu and its surface, V_{33}^{elect} is proportional, and with opposite sign, to V_{33}^{ionic} :

$$V_{33}^{elect} = -K(1 - \gamma_{\infty})V_{33}^{latt} \quad , \quad (2)$$

being K and γ_{∞} positive and negative numbers, respectively. In this case V_{33}^{tot} reduces to:

$$V_{33}^{tot} = (1 - K)(1 - \gamma_{\infty})V_{33}^{latt} = A_{Cu} V_{33}^{latt} \approx -2(1 - \gamma_{\infty})V_{33}^{latt} \quad (3)$$

In Eq. (3), we have used the fact that for many metallic impurity-host systems $K \approx +3$, in particular for small and medium values of V_{33}^{ionic} , but other metals showed $K \approx +2$. Hence, we can suppose that the conduction-electron contribution to the EFG may be dominant and representative of the total EFG. As we will discuss later, V_{33} “lattice” calculations at the surface (Cu_1 site) yield a negative value, hence the reversal sign of the universal correlation applies to this surface system, with a multiplicative coefficient $A_{Cu} = (1 - K)(1 - \gamma_{\infty})$ around twice or equal to that predicted by the Sternheimer antishielding factor [34]-[36]. On the other hand, the electron densities in Fig. 5 were constructed by filtering the partial density of states (PDOS) projected onto the Cu_1 atom over an energy range of 1.47 eV below the Fermi level, corresponding, as mentioned before, to the more energetic (conduction) electron.

In Fig. 6, we show the total DOS for the *reconstructed* Cu(100) surface at 300 K, the s -, p -, and d -PDOS projected onto Cu_1 , and a zoom-in on the p_z and p_x+p_y contributions at the topmost atom. Successive energy regions corresponding to the last, 2nd, and 3rd more energetic electrons are separated by vertical lines. The Cu_1 - p and Cu_1 - d contributions to the total EFG at the surface are positive and negative, respectively, with the p contribution dominant. The majority contribution to the EFG can be split in two parts [28], [27], [37], [18], V_{33}^p and V_{33}^d , proportional to the p and d asymmetry counts Δn_p and Δn_d , which are given in terms of the partial charges (occupation numbers) n_{p_i} and n_{d_i} of the corresponding l_i orbital:

$$\Delta n_p = \frac{1}{2}(n_{p_x} + n_{p_y}) - n_{p_z} \quad (4)$$

$$\Delta n_d = \left[(n_{d_{x^2-y^2}} + n_{d_{xy}}) \right] - \left[\frac{1}{2}(n_{d_{xz}} + n_{d_{yz}}) + n_{d_{z^2}} \right] \quad (5)$$

As seen in Fig. 6 (bottom), the energy region of the last electron reflects the positive character of the p contribution to V_{33} that holds across all energies, with the d contribution also (locally) positive in this small energy region. On the other hand, the magnitude of

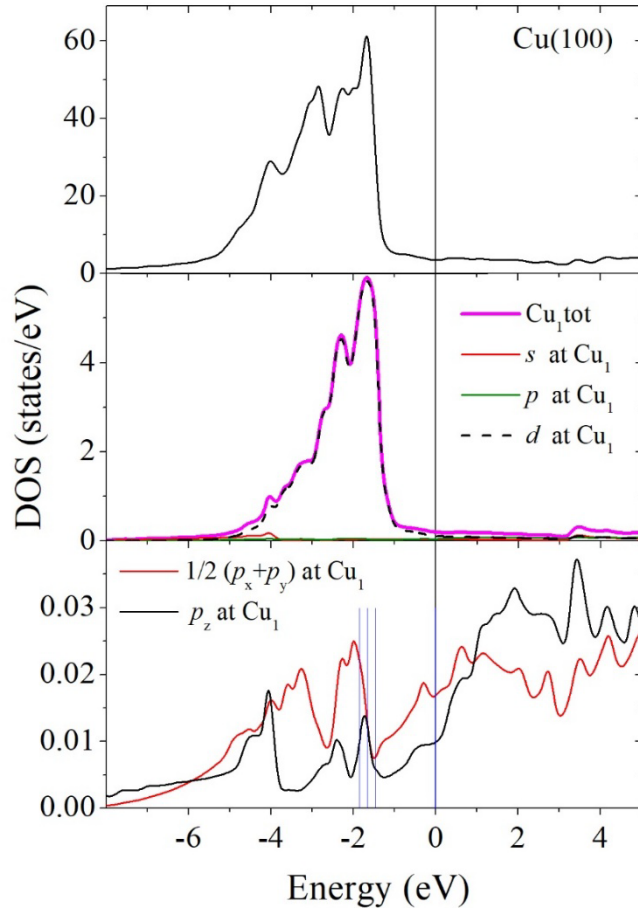


Figure 6. Electronic density of states (DOS) for the *reconstructed* Cu(100) surface at 300 K. Top: total DOS. Middle: s -, p -, and d -partial DOS projected onto Cu_1 . The p -contribution is nearly invisible on this scale. Bottom: zoom on the p_z and p_x+p_y contributions at this topmost atom. Energy is referenced to the Fermi level.

V_{33} depends mainly on the distance of the nonspherical source charges to the probe nucleus. In the Cu atom, the first node of the $3p$ wave function (and even more if $4p$ states are also populated in the solid) is at shorter distance than the one of the $3d$ wave function, according to the rule that the number of nodes is equal to $n-l-1$, resulting in a dominant p contribution to V_{33} even though the asymmetry count Δn_d may be larger than Δn_p . All these facts correlate perfectly with the angular shape of $\rho(\vec{r})$ shown in

Fig. 5 at Cu_1 and justifies the choice of this energy region to illustrate the origin of the *large* and *positive* EFG at the surface. On the contrary, for Cu atoms in bulk, all shells must be completely spherical due to the crystal symmetry (all occupation numbers n_{p_i} and n_{d_i} are equal to 2 in Eqs. 4 and 5), leading to a null V_{33} value.

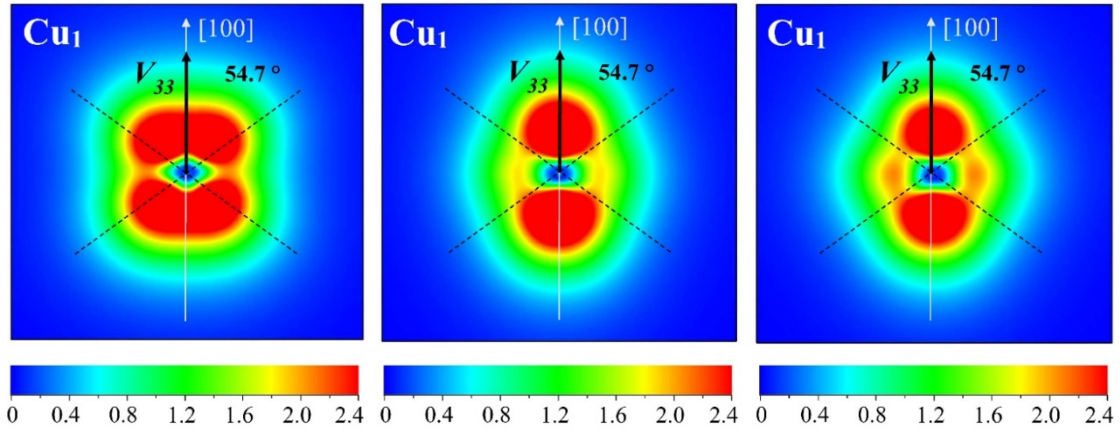


Figure 7. Electron density $\rho(\vec{r})$ in the (010) plane containing the topmost Cu_1 atom of the *reconstructed* Cu(100) surface, for the 2nd-most energetic electron (left), the 3rd-most energetic electron (middle), and the 4th-most energetic electron (right) at 300 K.

Figure 7 shows plots of $\rho(\vec{r})$ for the 2nd-, 3rd-, and 4th-most energetic electrons at the topmost Cu_1 . This sequence shows a transition from the electronic donut-like shape shown in Fig. 5 (left) at Cu_1 to geometries more and more aligned to the V_{33} axis, contributing with a negative sign to the EFG in these energy regions, in accordance with the large and increasing number of d -states in the PDOS as going to lower energies. For the 4th electron, a small density perpendicular to V_{33} is detected (Fig. 7, right), probably correlated with an increase in the occupation of the p_x and p_y states relative to the p_z states. Nevertheless, the close proximity of the asymmetric p -states to the nucleus and the near parity of the total d and p asymmetry counts across all energies ensure a positive EFG at the Cu(100) surface.

Now, we present the prediction of the EFG at the topmost Cu₁ atom ($V_{33}^{Surface}$) as a function of temperature. In Fig. 8, we plot our *ab initio* predictions for $V_{33}^{Surface}$ for both the *just-generated* and *reconstructed* Cu(100) surfaces.

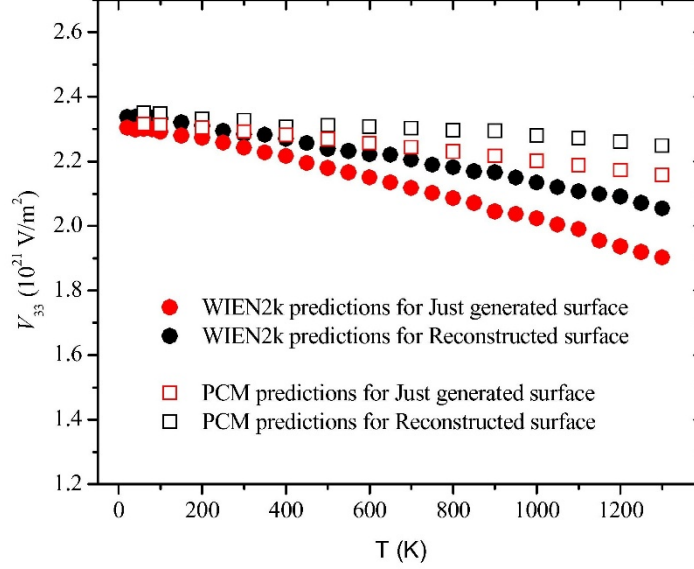


Figure 8. *Ab initio* predicted $V_{33}^{Surface}$ at the topmost Cu₁ atom for the *just-generated* and *reconstructed* Cu(100) surfaces, using Cu lattice parameters as a function of temperature. Open symbols are predictions of $V_{33}^{Surface}$ proposing a factorization as in Eq. (3): $V_{33}^{Surface}(T) = A_{Cu} \cdot V_{33}^{latt}(T)$, with the lattice contribution calculated using a point-charge model (PCM) considering first and second nearest neighbors from Cu₁.

In both cases (for the just-generated and the reconstructed surfaces), V_{33} varies almost linearly with temperature. When surfaces reach their equilibrium structures, the predicted V_{33} slope decreases slightly. Fitting both curves with $V_{33}(T) = a + m \cdot T = [V_{33}(0 \text{ K}) + m \cdot T] \times 10^{21} \text{ V/m}^2$ we found for the just-generated surface $V_{33}(0 \text{ K}) = 2.32$ and $m = -3.1 \times 10^{-4}$ (m/a= 0.013%), and for the reconstructed one $V_{33}(0 \text{ K}) = 2.35$ and $m = -2.21 \times 10^{-4}$ (m/a=0.0094%). For this temperature range, a linear fit to the V_{33} values reported by Klass *et al.* [10], using a quadrupole moment $Q = + 0.76(2) \text{ b}$ [38], gives: $V_{33}(0 \text{ K}) = 11.25(5)$ and $m = -11.8(5) \times 10^{-4}$ (m/a= 0.0104(5) %). This apparent coincidence in the m/a ratio is still a subject of study.

Analyzing this predicted behavior in the framework of Eq. 3, and calculating V_{33}^{latt} using a simple point-charge model (PCM) taking into account the first and second

nearest neighbors to the Cu₁ atom for both *just-generated* and *reconstructed* surfaces, using charge state q=1+ for all Cu ions in the lattice, we found a multiplicative constant $A_{Cu} \approx -10$, hence obtaining for the K parameter a value of 2 in this system. At this point, we can see that if V_{33}^{latt} is calculated taking into account more neighboring atoms, the *ab initio* predictions and the model proposed in Eq. 3 (filled circles and open squares in Fig. 8), could probably show better agreement. In effect, e.g., if V_{33}^{latt} at 0 K should be half the actual value and the slope m of its temperature dependence remains more or less the same, the slopes of the *ab initio* prediction and that of Raghavan's parametrization will match. Another possibility is that Eq. 3 needs an additional term also linearly dependent on T. Nevertheless, the qualitative agreement shown in Fig. 8 indicates that the linear dependence of $V_{33}^{Surface}$ with T is mainly due to the structural lattice behavior with T, already in the case of the *just-generated* surface, i.e., it seems that the (100) surface generation is responsible for the linear dependence on T of $V_{33}^{Surface}$. Also, it is apparent that the subsequent lattice relaxation decreases the slope of the linear T dependence.

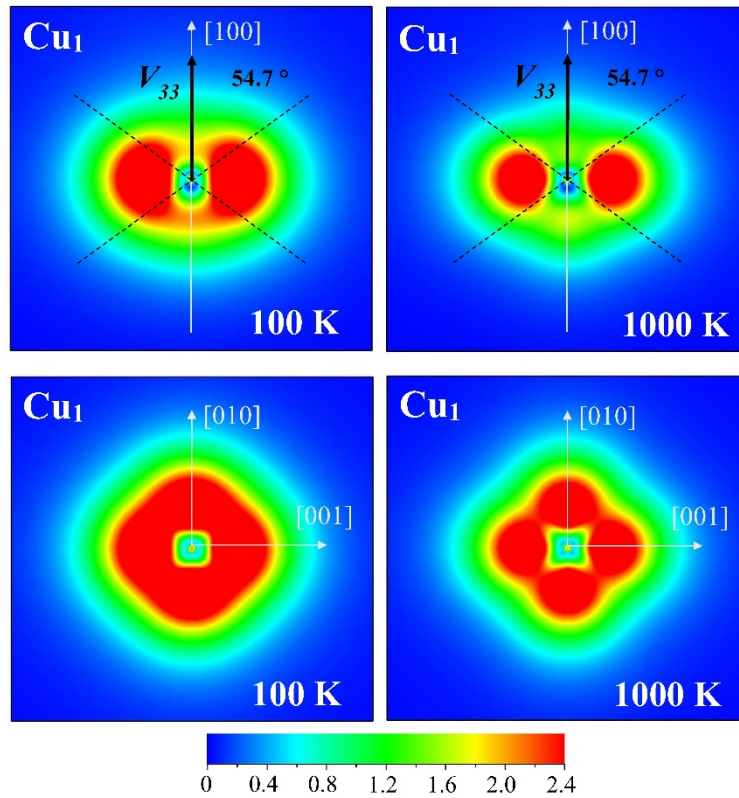


Figure 9. Electron density $\rho(\vec{r})$ at the (010) (up) and (100) (bottom) planes containing the topmost Cu_1 atom, for the most energetic (conduction) electron at 100 K and 1000 K.

Finally, the electron densities shown in Fig. 9 for the topmost Cu_1 atom, corresponding to the most energetic electron in the *reconstructed* surface, yield positive V_{33} values along the [100] axis at both temperatures, because the negative charge is mainly distributed closer to the (100) plane than to the V_{33} axis, as explained earlier. In addition, the magnitude of this charge's contribution to V_{33} decreases with increasing temperature. In effect, at 1000 K, the negative charge remains near the (100) plane but is substantially reduced relative to lower temperatures.

CONCLUSIONS

Applying state-of-the-art first-principles calculations, we study the Cu(100) surface reconstruction and its structural, electronic, and hyperfine properties as a function of temperature and depth from the surface.

Using experimentally determined temperature-dependent lattice parameters of copper, we studied the reconstructed surfaces, finding that the contraction of the topmost 1-2 interlayer distance and the expansion of the second 2-3 one relative to the bulk interlayer width are in excellent agreement with experimental results as a function of T, supporting the predicted reconstructed surfaces.

We found that the spatial redistribution of the electronic density of conduction electrons at the atomic scale near the nucleus of the topmost Cu₁ atom explains the surface effect on the large EFG value relative to the bulk value, and its decrease with increasing temperature.

We show that the linear decrease of the EFG as T increases, as evidenced by TDPAC experiments on the ¹¹¹Cd-doped Cu(100) surface, is probably mostly caused by the surface generation of pure Cu.

ACKNOWLEDGEMENTS

CONICET and UNLP partially supported this work under Research Grants No. PIP0901 and No. 11/X1004, respectively. This research used the computational facilities of the Physics of Impurities in Condensed Matter group at IFLP and at the Department of Physics (UNLP). G.N.D. and M.R. are members of CONICET, Argentina. R.F. acknowledges PEDECIBA, CSIC-UdelaR, and ANII, all Uruguayan Institutions for financial support.

Corresponding Authors

*E-mail: darriba@fisica.unlp.edu.ar ; reneria@fisica.unlp.edu.ar

REFERENCES

- [1] T. Zhang *et al.*, Experimental Demonstration of Topological Surface States Protected by Time-Reversal Symmetry, *Phys. Rev. Lett.* **103**, 266803 (2009).

- [2] T. Okuda *et al.*, Experimental Evidence of Hidden Topological Surface States in PbBi₄Te₇, *Phys. Rev. Lett.* **111**, 206803 (2013).
- [3] H.-J. Noh, J. Jeong, E.-J. Cho, J. Park, J. S. Kim, I. Kim, B.-G. Park, and H.-D. Kim, Controlling the evolution of two-dimensional electron gas states at a metal/Bi₂Se₃ interface, *Phys. Rev. B* **91**, 121110 (2015).
- [4] S. Schulz *et al.*, Classical and cubic Rashba effect in the presence of in-plane 4f magnetism at the iridium silicide surface of the antiferromagnet GdIr₂Si₂, *Phys. Rev. B* **103**, 035123 (2021).
- [5] C. Song *et al.*, Observation of spin-polarized surface states in the nodal-line semimetal SnTaS₂, *Phys. Rev. B* **107**, 045142 (2023).
- [6] H. Frauenfelder and R. M. Steffen, *Alpha-, Beta-, and Gamma-Ray Spectroscopy*, K. Seigbahn, Vol. 2 (North-Holland Publishing Co., Amsterdam, Netherlands, 1968).
- [7] E. N. Kaufmann and R. J. Vianden, The electric field gradient in noncubic metals, *Rev. Mod. Phys.* **51**, 161 (1979).
- [8] G. Schatz and A. Weidinger, *Nuclear Condensed Matter Physics: Nuclear Methods and Applications* (Wiley, Chichester, England, 1996).
- [9] G. N. Darriba, R. Faccio, P.-D. Eversheim, and M. Rentería, Insights on the relevance of DFT+U formalism for strongly correlated Ta-*d* electrons probing the nanoscale in oxides: Combined time-differential perturbed γ - γ angular correlation spectroscopy and *ab initio* study in ¹⁸¹Hf(\rightarrow ¹⁸¹Ta)-implanted α -Al₂O₃ single crystal, *Phys. Rev. B* **108**, 245144 (2023).
- [10] T. Klas, J. Voigt, W. Keppner, R. Wesche, and G. Schatz, Characterization of Copper (100) Surfaces by Isolated Indium Probe Atoms via the Electric Field Gradient, *Phys. Rev. Lett.* **57**, 1068 (1986).
- [11] T. Klas, R. Fink, G. Krausch, R. Platzter, J. Voigt, R. Wesche, and G. Schatz, Microscopic Observation of Step and Terrace Diffusion of Indium Atoms on Cu(111) Surfaces, *EPL* **7**, 151 (1988).
- [12] T. Klas, R. Fink, G. Krausch, R. Platzter, J. Voigt, R. Wesche, and G. Schatz, Isolated indium atoms on copper surfaces: A perturbed γ - γ angular correlation study, *Surface Science* **216**, 270 (1989).
- [13] R. Wesche, R. Fink, T. Klas, G. Krausch, R. Platzter, J. Voigt, and G. Schatz, The electric field gradient for single indium atoms on low-index silver surfaces, *J. Phys.: Condens. Matter* **1**, 7407 (1989).

- [14] E. Hunger and H. Haas, Adsorption sites and diffusion steps of In and Cd on Pd(111) surfaces, *Surface Science* **234**, 273 (1990).
- [15] R. Fink, R. Wesche, T. Klas, G. Krausch, R. Platzer, J. Voigt, U. Wöhrmann, and G. Schatz, Step-correlated diffusion of in atoms on Ag(100) and Ag(111) surfaces, *Surface Science* **225**, 331 (1990).
- [16] R. Fink, B.-U. Runge, K. Jacobs, G. Krausch, J. Lohmuller, B. Luckscheiter, U. Wöhrmann, and G. Schatz, Indium adsorption sites at Pd(100) surfaces studied by PAC spectroscopy, *J. Phys.: Condens. Matter* **5**, 3837 (1993).
- [17] K. Potzger, A. Weber, H. H. Bertschat, W.-D. Zeitz, and M. Dietrich, Coordination-Number Dependence of Magnetic Hyperfine Fields at $\{111\}$ Cd on Ni Surfaces, *Phys. Rev. Lett.* **88**, 247201 (2002).
- [18] S. Cottenier, V. Bellini, M. Çakmak, F. Manghi, and M. Rots, Coordination dependence of hyperfine interactions at impurities on fcc metal surfaces. I. Electric-field gradient, *Phys. Rev. B* **70**, 155418 (2004).
- [19] P. Jena, Temperature Dependence of Electric Field Gradients in Noncubic Metals, *Phys. Rev. Lett.* **36**, 418 (1976).
- [20] K. Wang and R. R. Reeber, Thermal expansion of copper, *High Temperature and Materials Science* **35**, 181 (1996).
- [21] P. Hohenberg and W. Kohn, Inhomogeneous Electron Gas, *Phys. Rev.* **136**, B864 (1964).
- [22] W. Kohn and L. J. Sham, Self-Consistent Equations Including Exchange and Correlation Effects, *Phys. Rev.* **140**, A1133 (1965).
- [23] G. K. H. Madsen, P. Blaha, K. Schwarz, E. Sjöstedt, and L. Nordström, Efficient linearization of the augmented plane-wave method, *Phys. Rev. B* **64**, 195134 (2001).
- [24] P. Blaha, K. Schwarz, G. Madsen, D. Kvasnicka, and J. Luitz, *WIEN2k, an Augmented Plane Wave Plus Local Orbitals Program for Calculating Crystal Properties* (Technical Universität, Wien, Austria, 2014).
- [25] J. P. Perdew, K. Burke, and M. Ernzerhof, Generalized Gradient Approximation Made Simple, *Phys. Rev. Lett.* **77**, 3865 (1996).
- [26] P. E. Blöchl, Projector augmented-wave method, *Phys. Rev. B* **50**, 17953 (1994).
- [27] K. Schwarz, C. Ambrosch-Draxl, and P. Blaha, Charge Distribution and Electric-Field Gradients in YBa₂Cu₃O_{7-x}, *Phys. Rev. B* **42**, 2051 (1990).

- [28] P. Blaha, K. Schwarz, and P. H. Dederichs, First-principles calculation of the electric-field gradient in hcp metals, *Phys. Rev. B* **37**, 2792 (1988).
- [29] D. E. Fowler and J. V. Barth, Structure and Dynamics of the Cu(001) Surface Investigated by Medium-Energy Ion Scattering, *Phys. Rev. B* **52**, 2117 (1995).
- [30] W. Körner, W. Keppner, B. Lehndorff-Junges, and G. Schatz, Sensitive Probing of Surfaces by Electric Quadrupole Interaction Demonstrated for Indium Metal, *Phys. Rev. Lett.* **49**, 1735 (1982).
- [31] G. N. Darriba, E. L. Muñoz, A. W. Carbonari, and M. Rentería, Experimental TDPAC and Theoretical DFT Study of Structural, Electronic, and Hyperfine Properties in (111In \rightarrow)111Cd-Doped SnO₂ Semiconductor: Ab Initio Modeling of the Electron-Capture-Decay After-Effects Phenomenon, *J. Phys. Chem. C* **122**, 17423 (2018).
- [32] R. S. Raghavan, E. N. Kaufmann, and P. Raghavan, Universal Correlation of Electronic and Ionic Field Gradients in Noncubic Metals, *Phys. Rev. Lett.* **34**, 1280 (1975).
- [33] P. Raghavan, E. N. Kaufmann, R. S. Raghavan, E. J. Ansaldo, and R. A. Naumann, Sign and magnitude of the quadrupole interaction of ¹¹¹Cd in noncubic metals: Universal correlation of ionic and electronic field gradients, *Phys. Rev. B* **13**, 2835 (1976).
- [34] H. M. Foley, R. M. Sternheimer, and D. Tycko, Nuclear Quadrupole Coupling in Polar Molecules, *Phys. Rev.* **93**, 734 (1954).
- [35] R. M. Sternheimer, Quadrupole Antishielding Factors of Ions, *Phys. Rev.* **159**, 266 (1967).
- [36] F. D. Feiock and W. R. Johnson, Atomic Susceptibilities and Shielding Factors, *Phys. Rev.* **187**, 39 (1969).
- [37] H. M. Petrilli and S. Frota-Pessoa, Calculations of the electric field gradient at the nucleus of an Fe impurity in HCP Zr by the recursion method, *J. Phys. F: Met. Phys.* **15**, 2307 (1985).
- [38] L. Errico, K. Lejaeghere, J. Runco, S. N. Mishra, M. Rentería, and S. Cottenier, Precision of Electric-Field Gradient Predictions by Density Functional Theory and Implications for the Nuclear Quadrupole Moment and Its Error Bar of the 111Cd 245 keV 5/2+ Level, *J. Phys. Chem. C* **120**, 23111 (2016).